Biomaterials Science

Delivery of 5'-Triphosphate RNA with Endosomolytic Nanoparticles Potently Activates RIG-I to Improve Cancer Immunotherapy

SCHOLARONE™
Manuscripts

Biomaterials Science

ARTICLE

Delivery of 5'-Triphosphate RNA with Endosomolytic Nanoparticles Potently Activates RIG-I to Improve Cancer Immunotherapy

Max Jacobson[1], Lihong Wang-Bishop[1], Kyle W. Becker[1], and John T. Wilson[1-5,*]

RNA agonists of the retinoic acid gene I (RIG-I) pathway have recently emerged as a promising class of cancer immunotherapeutics, but their efficacy is hindered by drug delivery barriers, including nuclease degradation, poor intracellular uptake, and minimal access to the cytosol where RIG-I is localized. Here, we explore the application of pH-responsive, endosomolytic polymer nanoparticles (NPs) to enhance the cytosolic delivery and immunostimulatory activity of synthetic 5' triphosphate, short, double-stranded RNA (3pRNA), a ligand for RIG-I. Delivery of 3pRNA with pH-responsive NPs with an active endosomal escape mechanism, but not control carriers lacking endosomolytic activity, significantly increased the activity of 3pRNA in dendritic cells, macrophages, and cancer cell lines. In a CT26 colon cancer model, activation of RIG-I via NP delivery of 3pRNA induced immunogenic cell death, triggered expression of type I interferon and pro-inflammatory cytokines, and increased CD8+ T cell infiltration into the tumor microenvironment. Consequently, intratumoral (IT) delivery of NPs loaded with 3pRNA inhibited CT26 tumor growth and enhanced the therapeutic efficacy of anti-PD1 immune checkpoint blockade, resulting in a 30% complete response rate and generation of immunological memory that protected against tumor rechallenge. Collectively, these studies demonstrate that pH-responsive NPs can be harnessed to strongly enhance the immunostimulatory activity and therapeutic efficacy of 3pRNA and establish endosomal escape as a critical parameter in the design of carriers for immunotherapeutic targeting of the RIG-I pathway.

Introduction

Immunotherapy with PD-1 immune checkpoint blockade (ICB) is transforming the treatment of an increasing number of cancers, resulting in complete and durable responses in a subset of patients.[1, 2] However, despite these unprecedented outcomes, the vast majority of patients do not respond to recently approved anti-PD-1 monoclonal antibodies (e.g., Pembrolizumab), motivating significant recent investigation into strategies to increase response rates to ICB.[3, 4] Anti-PD-1 antibodies act by blocking the interaction between PD-1 on the surface of tumor infiltrating T cells, and its ligand, PD-L1, expressed primarily on tumor cells and tumor-associated myeloid cells. Disrupting the PD-1/PD-L1 interaction disables this powerful immune checkpoint, reinvigorating anti-tumor T cell effector function and cytotoxic activity.[5] Accordingly, for many cancer types, response to PD-1 antibodies correlates with the relative abundance of tumor infiltrating T cells that are positioned to be reactivated in response to PD-1 blockade.[6, 7] However, many patients and/or cancer types lack this critical T cell-inflamed immunological signature, and instead have tumor microenvironments (TME) that are largely devoid of T cells and highly infiltrated immunosuppressive cell populations.[8, 9] This realization has motivated a need for immunotherapeutic modalities that can transform the TME into a hotbed of anti-tumor immune activity.

The innate immune system plays a critical role in mounting and shaping adaptive immune responses.[10] Accordingly, a variety of innate immune activators are now being explored clinically as therapeutics to abrogate immunosuppression in the TME while also creating an immunostimulatory milieu that supports the priming, activation, and infiltration of anti-tumor T cells.[11-14] The majority of these strategies leverage molecularly defined agonists of pattern recognition receptors (PRR), innate immune sensors that recognize unique structural motifs of pathogens or endogenous stress signals.[15] Notable examples include the toll-like receptor (TLR) 7 agonist, imiquimod, which has been approved for topical treatment of superficial basal cell carcinoma,[16] and the TLR-9 agonist, CpG ODN, which is approved as a vaccine adjuvant[17] and is being extensively explored in cancer

[1]Department of Chemical and Biomolecular Engineering; Vanderbilt University Nashville, TN 37235, USA

[2]Department of Biomedical Engineering; Vanderbilt University

[3]Vanderbilt Center for Immunobiology; Vanderbilt University

[4]Vanderbilt Institute for Infection, Immunology and Inflammation; Vanderbilt University

[5]Vanderbilt-Ingram Cancer Center; Vanderbilt University

*CORRESPONDING AUTHOR. John T. Wilson; Tel: +1-615-322-6406; e-mail: john.t.wilson@vanderbilt.edu

immunotherapy clinical trials.[18] While promising, the utility and efficacy of TLR ligands may be limited by the expression profile of TLRs, which are typically restricted to leukocytes and, in some instances (e.g., TLR-9), to specific immune cell subsets that may be infrequent or highly heterogeneous within and/or across tumors.[19] Moreover, while many PRRs share common signaling molecules, the molecular phenotype (e.g., cytokine profile) of the resultant innate immune response can vary significantly between PRRs, with attendant consequences on adaptive immunity.[15, 20, 21] Recent studies have demonstrated that a type-I interferon (IFN) gene expression signature correlates with T cell infiltration into melanoma metastases and improved response to ICB, providing rationale for design and use of PRR agonists that stimulate type-I IFN and interferon stimulated genes (ISGs) implicated in endogenous anti-tumor immunity (e.g., CXCL9,10).[12, 22, 23] Interestingly, anti-tumor innate immunity appears to have considerabe homology with innate responses that occur during viral recognition and defence, and indeed, a growing body of evidence now implicates PRR sensing of endogenous retroviral elements in stimulation of anti-tumor immunity.[24, 25]

Retinoic acid inducible gene I (RIG-I) is an important PRR for viral sensing that potently activates antiviral innate immunity upon recognition of 5' di- or tri-phosphorylated (2p- or 3pRNA) short, double-stranded RNA in the cytosol.[26-29] Unlike the TLRs, RIG-I is present in the cytosol of virtually all cell types, including tumor cells, potentially rendering it a more universal innate immune target for cancer immunotherapy that is less dependent of the presence of specific infiltrating immune cell populations.[30-33] Additionally, activation of RIG-I signaling has been shown to induce preferential apoptosis in several cancer cells, whereas nonmalignant cells, notably antigen presenting cells, are more resistant to RIG-I-mediated apoptosis.[33-35] Therefore, in addition to activating a multipotent IFN-I-driven inflammatory response, cancer cell death triggered by RIG-I signaling could liberate tumor antigen, potentially enhancing cross presentation and priming of anti-tumor T cells.[36-39] Consequently, RIG-I has recently emerged as a promising target in immuno-oncology, with 3pRNA RIG-I agonists currently being explored in clinical trials (e.g. NCT03065023).

While RNA RIG-I agonists are a promising class of immunotherapeutic, they face multiple barriers to efficacy that are shared with other nucleic acid therapeutics (e.g., siRNA), including nuclease degradation, poor intracellular uptake, and critically, endo/lysosomal degradation with minimal cytosolic delivery.[40, 41] While there has been extensive work for developing systems for siRNA, mRNA, and DNA delivery,[42, 43] including polyplexes, inorganic nanoparticles, and lipid-based nanomaterials, to name few, there has been minimal investigation into delivery systems for RIG-I agonists. Indeed, the majority of studies exploring mechanisms or applications of RIG-I ligands have utilized commercial *in vitro* lipid-based transfection agents or polyethylenimine (PEI),[27, 39, 44] which has been widely explored for nucleic acid delivery, but has not been optimized for 2p- or 3pRNA delivery nor approved for human use, despite decades of research and development. Hence, to harness the immunotherapeutic potential of the RIG-I pathway, there is a need to explore and develop new delivery platforms for 2p- and 3pRNA as well as to establish carrier design criteria for this unique and emergent class of RNA therapeutic.

Owing to the dearth of carrier technologies for 3pRNA, we sought to evaluate the ability of a pH-responsive, membrane destabilizing polymeric nanoparticle (NP) to enhance the cytosolic delivery and immunotherapeutic activity of a synthetic 3pRNA RIG-I ligand.[45-47] These NPs are composed of amphiphilic diblock copolymers with a cationic dimethylaminoethyl methacrylate (DMAEMA) first block for facile electrostatic complexation and protection of nucleic acid cargo, and an endosome-destabilizing terpolymer block comprising DMAEMA, butyl methacrylate (BMA), and propylacrylic acid (PAA), that act cooperatively to mediate efficient cytosolic delivery (Figure 1a). This platform, and variants thereof, has been used previously to enhance intracellular delivery of siRNA and proteins,[47-50] but has not been explored for immunotherapeutic applications of 3pRNA delivery. Here, we evaluate the ability of endosomolytic NPs to enhance the immunostimulatory potency of 3pRNA, to stimulate RIG-I activation in the TME, and to improve responses to PD-1 checkpoint blockade.

Experimental

RAFT Polymerization of p(DMAEMA)-*b*-(DMAEMA-*co*-BMA-*co*-PAA). Briefly, Inhibitor was removed from all monomer solutions used for RAFT polymerization using gravity filtration through columns packed with aluminum oxide (Sigma Aldrich). RAFT polymerization of dimethylaminoethyl methacrylate (DMAEMA) (Sigma Aldrich) was conducted under a nitrogen atmosphere in dioxane (40 wt % monomer) at 30°C for 18 h in the presence of 4-cyano-4-(ethylsulfanylthiocarbonyl)sulfanylpentanoic acid (ECT) (Boron Molecular) and 2,20-azobis(4-methoxy-2.4-dimethyl valeronitrile) (V-70) (Wako Chemicals) as the RAFT chain transfer agent and initiator, respectively. The initial monomer (M_o) to CTA (CTA_o) to initiator (I_o) ratio was 100:1:0.05. The resultant p(DMAEMA)) macro-chain transfer agent (mCTA) was isolated by precipitation into cold pentane. The mCTA was transferred to a 3 kDa MWCO snakeskin dialysis membrane (Thermo Fisher) and exchanged into 2L of molecular grade water (HyClone) twice for 6 h. The solution was frozen, lyophilized, and characterized using ^{1}H nuclear magnetic resonance (NMR) (Bruker AV 400) and gel permeation chromatography (GPC) (Agilent). Propylacrylic acid (PAA) was synthesized as described previously using diethyl propylmalonate (Sigma Aldrich) as the precursor.[51] Purified mCTA was used for block copolymerization of DMAEMA, (PAA), and butyl methacrylate (BMA) (Sigma Aldrich) or BMA only. DMAEMA (30%), PAA (30%), and BMA (40%), or BMA (100%) (M_o/CTA_o = 0.2) were added to the mCTA dissolved in dioxane (40 wt % monomer and mCTA) along with the free radical initiator V-70 at a mCTA to initiator ratio ($mCTA_0/I_0$) of 5 and polymerized under a nitrogen atmosphere for 24 h at 30 °C. The resultant diblock copolymer was isolated using dialysis (3kDa MWCO) against acetone (4 exchanges) with a final dialysis against molecular grade water (HyClone). The same process was used for the synthesis of p(DMAEMA)-*b*-p(BMA) (D-B), except the monomer feed only contained BMA. The purified polymer was then frozen and lyophilized. The composition and purity of the resultant polymer was analyzed using ^{1}H NMR and GPC. Polymer composition, purity, and molecular weight were determined using ^{1}H NMR (CDCl3) spectroscopy (Figure S1), and polymer molecular weight (Mn) and polydispersity (PDI) was determined using GPC using a DMF mobile phase with 0.1 M LiBr with inline light scattering (Wyatt) and refractive index (Agilent) detectors.

Synthesis of 5'-Triphosphate RNA. 5'-ppp-CGUUAAUCGCGUAUAAUACGCCUAU-3' was generously synthesized and provided by the laboratory of Dr. Anna M. Pyle at Yale University.[52] 5'-OH-CGUUAAUCGCGUAUAAUACGCCUAU-3' as well as the complement strand 5'-AUAGGCGUAUUAUACGCGAUUAACG-3' was purchased from Integrated DNA technologies (IDT) and resuspended in RNAse free water. To generate double stranded RNA, equimolar amounts of top strand with a triphosphorylated or OH 5' terminus top strand, and the complement strand were suspended in 0.3 M NaCl, transferred to a 0.25mL PCR tube and annealed using a thermocycler by setting the temperature to 90°C and slowly cooling to 35°C over 1 h. The resulting duplexes were diluted to 100µM RNA in RNAse free water and agarose gel (2%) electrophoresis was used to confirm hybridization.

Formulation of NP/3pRNA complexes for *in vitro* investigations. Amphiphilic diblock copolymer comprising a 10.3 kDa first block of DMAEMA and a 31.0 kDa second block copolymer of 33% DMAEMA, 39% butyl methacrylate (BMA), and 28% propylacrylic acid (PAA) (D-PDB) was synthesized as described above. Lyophilized copolymers were dissolved into ethanol at 50 mg/mL, and rapidly diluted into phosphate buffer (pH 7.0, 100 mM) to a final concentration of 10 mg/mL. This stock was further diluted to 1 mg/mL in phosphate buffered saline (155 mM NaCl, 1.05 mM KH_2PO_4, 3 mM Na_2HPO_4, Gibco), and rapidly mixed with either 3pRNA or OH-RNA at charge ratios (N:P) between 16:1 and 1:1, incubated at room temperature for 30 min, and diluted into PBS (pH 7.4, Gibco) in order to form nanoparticles (NPs). The first block of DMAEMA is estimated to have 50% protonation for the purposes of determining N:P ratios. A charge ratio of 4:1 was selected for all *in vitro* cell culture studies.

Dynamic Light Scattering. D-PDB (1 mg/mL) was mixed with OH-RNA as detailed above at a 4:1 charge ratio, and NP particle size distribution and polydispersity index (PDI) was analyzed via dynamic light scattering (Malvern Zetasizer Nano ZS).

Agarose Gel Electrophoresis. D-PDB (1 mg/mL) was mixed with OH-RNA as detailed above, except that the components were mixed at charge ratios of either 1:1, 2:1, 4:1, 8:1, or 16:1 resulting in a 15 µL NP solution comprising at least 100ng RNA. NP/RNA complexes and free RNA were mixed with 5 µL of 30% glycerol and loaded onto a 2% agarose gel. The gel was run in Tris-Borate-EDTA buffer at 100V for 60 min. The gel was stained with GelRed (Biotium) for 20 min and imaged using a Digital ChemiDoc MP system (Bio-Rad).

Red Blood Cell Hemolysis assay. All experiments using human samples were performed in compliance with United States Federal Policy for the Protection of Human Subjects and guidelines set forth by the Vanderbilt University Human Research Protections Program. These experiments were approved by the Vanderbilt University Institutional Review Board and consent was obtained from human subjects prior to all experimentation. The ability of NPs to disrupt lipid bilayer membranes was performed as previously described.[45] Whole blood from de-identified patients was acquired from the Vanderbilt Technologies for Advanced Genomics (VANTAGE) core. Blood was centrifuged at 500 rcf to pellet erythrocytes, and plasma was aspirated before resuspending erythrocytes in pH 7.4 PBS (Gibco). This process was repeated 3x to isolate erythrocytes, which were

ultimately resuspended in pH 7.4, 7.0, 6.6, 6.2, or 5.8 PBS (150 nM) for the hemolysis assay. D-PDB and D-B were mixed with suspended erythrocytes to a concentration of 10 µg/mL in a 96-well V-bottom plate. The plates were incubated for 1 h at 37°C, then centrifuged at 700 rcf to pellet intact erythrocytes. The supernatant was then transferred to a 96-well flat bottom plate and hemoglobin leakage was quantified by measuring absorbance at 575 nm.

Cell lines and Primary Bone Marrow-Derived Cells. The human lung carcinoma IRF and NF-κB reporter cell line A549-Dual (Invivogen) and the murine macrophage cell line RAW 264.7 (ATCC) was cultured in DMEM (Gibco) supplemented with 2mM L-glutamine, 4.5 g/L D-glucose, 10% heat inactivated fetal bovine serum (HI FBS, Gibco), and 100U/mL penicillin/100 µg/mL streptomycin (Gibco). The murine colon carcinoma CT26 cell type (ATCC), the murine breast cancer cell line 4T1 (ATCC), the human monocyte IRF and NF-κB reporter cell type THP1-Dual (Invivogen), and the murine melanoma cell type B16-F10 (ATCC) were cultured in RPMI 1640 (Gibco) supplemented with 2 mM L-glutamine, 10% fetal bovine serum (FBS, Gibco), and 100U/mL penicillin/100 µg/mL streptomycin (Gibco). The murine dendritic cell line DC2.4 (H-2K[b]-positive) was kindly provided by K. Rock (University of Massachusetts Medical School) and cultured in RPMI 1640 (Gibco) supplemented with 10% fetal bovine serum (HI FBS; Gibco), 2 mM L-glutamine, 100 U/mL penicillin/100 µg/mL streptomycin (Gibco), 50 µM 2-mercaptoethanol (Gibco), 1 × nonessential amino acids (Cellgro), and 10 mM HEPES (Invitrogen).

Bone marrow cells were isolated from both the femurs and tibias of 8–12 week old female wild-type BALB/cJ mice. After muscle tissue removal and ethanol sterilization of the bones, bone marrow was flushed out over a strainer with Dulbecco's phosphate-buffered saline (DPBS; Corning). Harvested cells were then rinsed with DPBS, erythrocytes were lysed using ACK Lysis buffer, (Gibco) and wells were resuspended in growth medium RPMI-1640 (Gibco) supplemented with 10% FBS (Gibco), 1% Penicillin Streptomycin (Gibco), 10 mM HEPES (Gibco), 1X nonessential amino acids (Sigma-Aldrich), 1 mM sodium pyruvate (Gibco), 55 µM 2-mercaptoethanol (Sigma-Aldrich), 50 µg/mL Gentamycin (Life Technologies), 2.5 µg/mL Amphotericin B (Corning) and 10 ng/mL Granulocyte-macrophage colonystimulating factor (GM-CSF, Peprotech) or RPMI-1640 (Gibco) supplemented with 10% FBS, 1% Penicillin Streptomycin (Gibco), 10 mM HEPES, 1X nonessential amino acids (Sigma-Aldrich), 1 mM sodium pyruvate (Gibco), 55 µM 2-mercaptoethanol (Sigma-Aldrich), 50 µg/mL Gentamycin (Life Technologies), 2.5 µg/mL Amphotericin B (Corning) and macrophage colony stimulating factor (M-CSF, Peprotech). BMDCs and BMDMs emerging from this were cultured and supplemented with additional supplemented RPMI-1640 on days 3 and 7 and were employed in experiments on days 8 to 12 after harvest. All cell types were grown in a humidified atmosphere with 5% CO_2 at 37 °C.

***In vitro* Evaluation of NP Delivery of 3pRNA.** For all cell lines, 5,000 cells were plated into 96-well plates and were allowed to adhere overnight for reporter cell activity or IFN-α secretion at multiple doses. CT26 cells were plated at 50,000 cells/well for PCR, flow cytometry, and HMGB1 concentration determination experiments. For BMDCs and BMDMs, 500,000 cells were plated in a 6-well plate and were adhered overnight for PCR and IFN-α concentration

determination experiments. After letting the cells adhere, cell supernatant was replaced with formulation diluted into fresh media at the indicated concentration. After 6 h or 24 h, the cell supernatant was collected for analysis and stored at -80 °C until used. For qRT-PCR analyses, cells were washed and 700 μL of RLT lysis buffer (Qiagen) was added to each well. Lysates were stored at -80 °C until used.

To determine the half maximal response concentration (EC$_{50}$) of indicated formulation, RNA dose sweeps between 0.05-50 nM final RNA concentration were performed in A549-Dual and THP1-Dual cell lines. Values for EC$_{50}$ were extrapolated from dose-response curve fits using GraphPad Prism software. NPs were formulated as detailed above and treated with D-PDB and 3pRNA (NP/3pRNA), D-PDB and OH-RNA (NP/OH-RNA), or D-B and 3pRNA (NP$_c$/3pRNA). Luminescent reporter assays were performed using QUANTI-Luc (Invivogen) following the manufacturer's instructions. Luminescence was quantified using a Synergy H1 microplate reader (BioTek, Winooski, VT). All measurements were normalized after baselining to the average value of the PBS-treated negative control group.

All other cell lines, as well as BMDCs and BMDMs, were treated with NPs at a 50nM final RNA concentration. Cells were treated with NPs formulated as detailed above, consisting of the following groups NP/3pRNA, NP/OH-RNA, D-PDB + PBS (NP only), and PBS. IFN-α concentrations in cell supernatant were determined using a Lumikine mIFN-α kit (Invivogen) according to the manufacturer's instructions. HMGB1 concentrations in cell supernatant were determined using an HMGB1 ELISA mouse kit (Cloud-Clone). mRNA was extracted from cell lysates using an RNA isolation kit (RNeasy mini kit, Qiagen). cDNA was synthesized for each sample using a cDNA synthesis kit (iScript, Bio-Rad) and analyzed using qRT-PCR using SybrGreen (Thermo Fischer) with CFX real time PCR detection system (Bio-Rad) following the manufacturer's instructions. Primers for *Ifnb1* (Mm.PT.58.30132453.g), *Cxcl10* (Mm.PT.58.4357827), *Il6* (Mm.PT.58.10005566), *Tnfa* (Mm.PT.58.12575861), and *Ppib* (Mm.PT.58.29807961) were purchased from Integrated DNA Technologies.

Protein Immunoblot. Cells were scraped on ice, centrifuged, and pellets were re-suspended in RIPA lysis buffer (Santa Cruz). Cell lysates were placed on ice. Protein concentration was measured using Pierce™ BCA Protein Assay Kit (Thermo Scientific, Waltham, PA). Equal amount of proteins were subjected to SDS-PAGE and transferred onto nitrocellulose membranes using the semi-dry transfer protocol (Bio-Rad Laboratories, Hercules, CA). After transfer, membranes were probed with primary antibodies for cleaved caspase 8 (9429T, Cell Signaling Technology), cleaved caspase 3 (9664T, CST), caspase 8 (9427T, CST), caspase 3 (SC 56053, Santa Cruz), phosphor-IRF3 (4997S, CST), IRF3 (4302S, CST), RIG-I (3743S, CST), phospo-STAT1 (9167S, CST), and β-actin (A5411, Sigma-Aldrich) overnight at 4°C. Following incubation, the membranes were probed with anti-mouse (W402B) or anti-rabbit (4401B) HRP-conjugated secondary antibodies (Promega). Protein bands were visualized using the commercial Immobile Western Chemiluminescent HRP Substrate Kit (Millipore, Billerica, MA). Images of immunoblots were obtained using the ChemiDoc XRS+ system (Bio-Rad).

Flow Cytometry. CT26 cells were plated and treated with indicated formulations as described above. After 24 h of treatment, supernatant was collected and cells were removed using 0.05% Trypsin-EDTA

(Gibco). Cells and supernatant were spun down and washed 3x in FACS buffer (0.5% BSA in PBS). Cells were stained with anti-calreticulin (AF647, ab196159, Abcam) and analyzed using a Guava easycyte HT benchtop flow cytometer (Millipore).

BMDM and BMDCs were plated and treated with indicated formulations as described above. After 24 h of treatment, cells were washed, removed from the plate using a cell scraper, pelleted via centrifugation (850 rcf, 5 min), and stained with a cocktail of anti-CD40-(FITC), CD80 (APC), and CD-86 (PE/Cy7) antibodies (BioLegend) in FACS buffer (0.5% BSA in PBS). DAPI staining was used to discriminate live from dead cells. Samples were kept on ice and analyzed using a BD-LSR Fortessa flow cytometer. All flow cytometry data were analyzed using FlowJo version 10 (Tree Star Inc).

Preparation of NP/3pRNA for *in vivo* studies. Polymer was dissolved in PBS as described above and subsequently buffer exchanged and concentrated into phosphate buffered saline (155 mM NaCl, 1.05 mM KH$_2$PO$_4$, 3 mM Na$_2$HPO$_4$, Gibco) via centrifugal dialysis following the manufacturer's instructions (Ambion, 3kDa MWCO, Millipore) and sterile filtered using a 0.22 μm syringe filter (Pall corporation) to 30-60 mg/mL. Final polymer concentration was determined spectrophotometrically (Synergy H1 microplate reader, BioTek) using an absorbance at 310 nm. Concentrated polymer solution was rapidly mixed with either 3pRNA or OH-RNA at a charge ratio of 4:1 (N:P), incubated at room temperature for 30 min, and diluted into PBS (pH 7.4, Gibco) prior to intratumoral (IT) administration.

Animal Care and Experimentation. Female BALB/cJ mice (7-11 weeks old) were obtained from The Jackson Laboratory (Bar Harbor, ME). All animals were maintained at the animal facilities of Vanderbilt University under specific pathogen-free conditions. All animal experiments were approved by the Vanderbilt University Institutional Animal Care and Use Committee (IACUC). Tumor volume, as well as mouse weight, was measured every other day via caliper measurements and a balance. Tumor volume was calculated using the equation $V = \frac{1}{2}(L * W * H)$.[53]

qRT-PCR Analysis of CT26 Tumors. Female BALB/cJ mice (11 weeks old mice) were inoculated with 100 μL of CT26 cells suspended in cold PBS (pH 7.4, Gibco), at 2x10^6 cells/mL. Once tumor volumes reached approximately 100 mm^3, Mice were intratumorally administered 50 μL of indicated formulation or vehicle (PBS) containing 25 μg of either 3pRNA or OH-RNA and 400 μg of polymer in PBS using a 0.5 cc syringe and a 29 gauge needle (n=4 for each group). The mice were treated once more 48 h after the first injection with the same formulation. After 24 h, mice from each group were euthanized, and tumors were surgically removed and stored at -20°C in RNA later. Tumors stored in RNA later were transferred into 1 mL of RLT lysis buffer in gentleMACs P tubes (Miltenyi Biotec) and digested using gentleMACS Octo dissociator (Miltenyi Biotec). Supernatant was transferred to RNAeasy mini columns for mRNA purification following the manufacturer's instructions. cDNA synthesis and qRT-PCR was performed as described above.

Immunoblot Analysis of CT26 Tumors. CT26 tumors were established subcutaneously in BALB/cJ mice and treated as described above. After 24 h, mice from each group were euthanized, and tumors were

surgically removed and stored at -20°C. For protein isolation, tumors stored dry at -80°C were transferred into 1mL of RIPA lysis buffer (Santa Cruz) in gentleMACs P tubes (Miltenyi Biotec) and digested using gentleMACS Octo dissociator (Miltenyi Biotec). Following centrifugation (2000 rcf, 3 min), supernatant was transferred to 2mL microcentrifuge tubes (Eppendorf). Protein immunoblotting was performed following the protocol described above.

Immunohistology of CT26 Tumors. CT26 tumors were established subcutaneously in BALB/cJ mice and treated as described above. After

24 h, mice from each group were euthanized, and tumors were surgically removed and stored in 10% formalin at room temperature. Tumors fixed in 10% formalin were paraffin embedded, sectioned, and sections were stained with hematoxylin and eosin. Immunohistochemistry was performed using the following antibodies: anti-Ki67 (Catalog #12202S, Cell Signaling Technology, Danvers, MA) and anti-CD8 (cat#14-0808-80, eBioscience Inc, San Diego, CA). Briefly, heat induced antigen retrieval was performed on the Bond Max using their Epitope
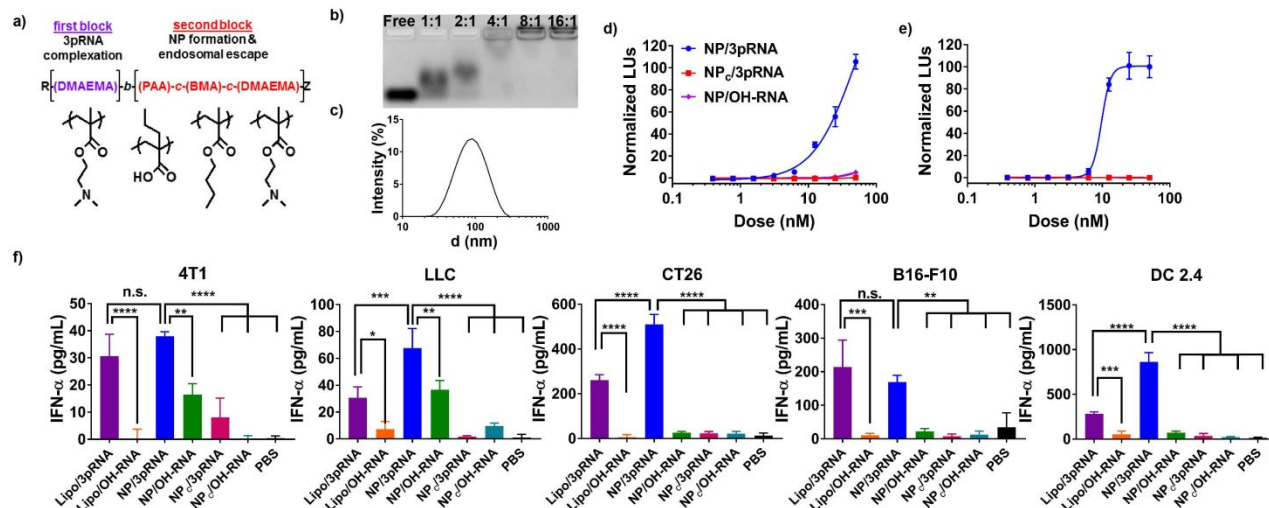
Figure 1: Endosomolytic nanoparticles enhance the delivery of 3pRNA to activate RIG-I pathway. (a) Schematic describing the structure and composition of pH-responsive, endosomolytic polymers used for 3pRNA delivery (NPs). The polymer consists of a poly(DMAEMA) first block for electrostatic complexation of 5' triphosphate double-stranded RNA (3pRNA) and a second terpolymer block responsible for assembly of micellar nanoparticles and inducing endosomal escape. (b) 3pRNA was incubated with NP at different charge ratios (N:P) and agarose gel electrophoresis used to evaluate the degree of nucleic acid complexation. (c) Dynamic light scattering analysis of particle size distribution of NP complexed with OH-RNA at N:P 4:1 (n=3). (d) THP1-Dual cells and (e) A549-Dual cells were treated with either NPs loaded with 3pRNA (NP/3pRNA) or OH-RNA (NP/OH-RNA), or non-pH-responsive NPs (NP$_c$) loaded with 3pRNA (NP$_c$/3pRNA) and activation of IRF was measured through secreted luciferase reporter levels. Luminescence was normalized using PBS treated samples and 100 nM NP/3pRNA treated samples (n=4). (f) Different cell types were treated with Lipofectamine (Lipo), NP, or NP$_c$ complexed with either 3pRNA or OH-RNA at final RNA doses of 50nM (n=3) and ELISA used to quantify levels of secreted IFN-α.

Retrieval 2 solution for 20 min. Slides were placed in a Protein Block (Ref# x0909, DAKO, a, CA) for 10 min. The sections were incubated with anti-Ki67 at a 1:300 dilution for 1 h. Sections were incubated with anti-CD8 at a dilution of 1:1500 for 1 h and then incubated in a rabbit anti-rat secondary (BA-4001, Vector Laboratories, Inc.) for 15 min at a 1:200 dilution. The Bond Refine Polymer detection system was used for visualization. Slides were then dehydrated, cleared and cover-slipped. Tumor sections were processed for this study using the translational pathology shared resource (TPSR) core facility at Vanderbilt University.

After processing, a minimum of four images of each sample were taken using a Leica DM2500 microscope. The percent positive cell populations were calculated using ImageJ cell counter tool. The population of Ki67+ and CD8+ cells were compared to the population of hematoxylin and eosin stained cells in each captured slide image.

Evaluation of NP/3pRNA in CT26 colon cancer model. Female BALB/cJ mice (7 weeks old) were inoculated with 100 µL of CT26 cells

suspended in cold PBS (pH 7.4, Gibco), at 10^6 cells/mL on day -12. On day 0, mice were administered 50 µL of NP/3pRNA or NP/OH-RNA at a dose corresponding to 25 µg RNA and 400 µg polymer in PBS every 2 days for 12 days. PBS was used as the vehicle control. In some cohorts, mice were administered 100 ug αPD1 (RMP1-14, BioXCell) in 100 uL PBS intraperitoneally every 4 days for 12 days. The groups for this study were the following: NP/3pRNA + αPD-1 (n=10), NP/3pRNA (n=10), NP/OH-RNA (n=8), PBS + αPD-1 (n=10), and PBS (n=10). Mice were euthanized when tumor volumes exceeded 1500 mm³.

Statistics. Significance was determined using one-way ANOVA with Tukey's multiple comparisons test unless otherwise noted. Values represent experimental means, and error bars represent S.E.M. unless otherwise noted. **** $p<0.0001$, *** $p<0.005$, **$p<0.01$, * $p<0.05$

Results and Discussion

Endosomolytic nanoparticles increase the immunostimulatory activity of 3pRNA. Towards developing a nanoparticle platform for

potent RIG-I activation, we first evaluated the ability of pH-responsive, membrane destabilizing DMAEMA-*b*-(DMAEMA-*c*-BMA-*c*-PAA) nanoparticles (NP) to enhance the immunostimulatory activity of a synthetic 3pRNA RIG-I ligand (Figure 1a). To determine the charge ratio needed to fully complex 3pRNA, polymeric NPs were complexed with different amounts of 3pRNA corresponding to various charge ratios of positively charged nitrogen to negatively charged phosphate (N:P ratio) ranging from 1:1 to 16:1, and agarose gel electrophoresis was used to evaluate complexation efficiency. Complete RNA complexation was achieved at a charge ratio of 4:1 (Figure 1b), which was selected for all subsequent investigations. We further confirmed assembly of polyplex nanoparticles at this charge ratio via dynamic light scattering, which demonstrated a monodisperse particle size

distribution with a median diameter of 108.5 nm and a polydispersity index (PDI) of 1.170 (Figure 1c).

We next evaluated 3pRNA activity in A549 human lung carcinoma cells and THP-1 monocyte ISG reporter cells that express a secreted luciferase downstream of an interferon response element.NPs loaded with control 5'-OH-RNA lacking a triphosphate group (OH-RNA) were used as a control to validate RIG-I dependent expression of ISGs. Additionally, since carriers for 3pRNA explored to date have not utilized an active endosomal escape mechanism, relying primarily on the proton sponge effect, we also sought to determine if the endosomolytic properties of the NP were critical to enhanced activity. To do this, we synthesized a structurally analogous diblock polymer with a DMAEMA first block and a
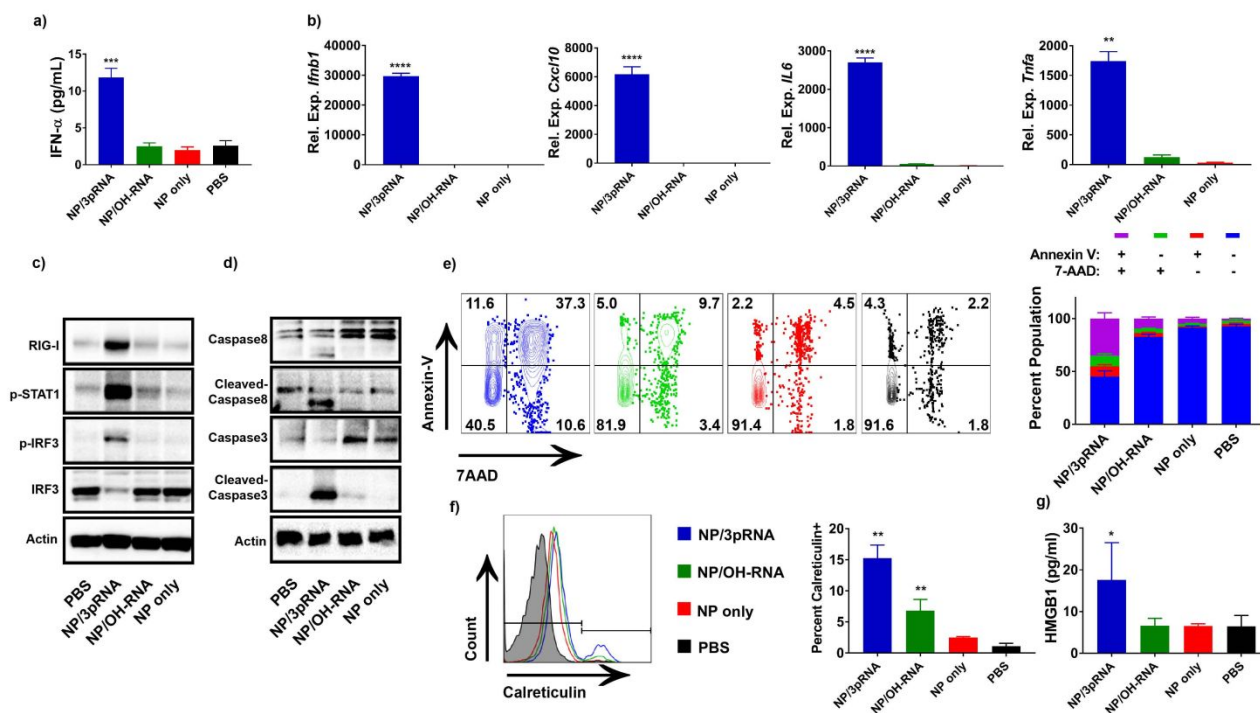
Figure 2: **NP delivery of 3pRNA induces production of inflammatory cytokines and mediates immunogenic cell death in CT26 cells.** (a) Levels of secreted IFN-α measured using ELISA after 24 h treatment of CT26 cells with indicated formulation (n=4). (b) qRT-PCR analysis of *Ifnb1*, *Cxcl10*, *Il6*, and *Tnfa* relative expression (Rel. Exp.) in CT26 cells treated with indicated formulation for 6 h (n=4). Representative images of western blots stained for (c) RIG-I, phosphorylated STAT1 (p-STAT1), and phosphorylated interferon regulatory factor 3 (p-IRF3) and (d) caspase 3 and caspase 8 cleavage in CT26 cells in response to indicated treatment for 24 h (n=3). (e) Representative flow cytometry dots plots and analysis of CT26 cell viability and apoptosis via annexin-V and 7-AAD staining after treatment with indicated formulation for 24 h. (f) Flow cytometry was used to determine cell surface levels of calreticulin on CT26 cells after indicated treatment for 24 h. Representative histogram and analysis of percent calreticulin positive cells are shown (n=4). (g) HMGB1 release from CT26 cells treated for 24 h was determined using ELISA (n=4). For NP/3pRNA, significance is between all other samples, and for NP/OH-RNA significance is between NP only and PBS.

poly(BMA) second block that is not pH responsive (Figure S3a, S3b) and that lacks hemolytic activity, which has been shown to correspond to endosomolytic activity (Figure S3c).[54] 3pRNA-loaded NPs (NP/3pRNA) exhibited an EC$_{50}$ between 10 nM and 20 nM for both cell types, while no activity was observed for 3pRNA complexed with the non-pH-responsive control nanoparticle (NP$_c$) over this dose range (Figure 1d, Figure 1e). Free 3pRNA that was

not bound to NP or lipofectamine was inactive over this dose range, consistent with poor cytosolic bioavailability of RNA therapeutics (Figure S4). In addition, NP delivery of OH-RNA (NP/OH-RNA) did not exhibit activity, confirming the 5'-triphosphate-dependent nature of

the response. These findings demonstrate the potential to leverage DMAEMA-*b*-(DMAEMA-*c*-BMA-*c*-PAA) polymeric NPs for 3pRNA delivery and support the importance of a potent endosomal escape mechanism in the design of carriers for RNA RIG-I ligands.

NP delivery of 3pRNA triggers inflammatory cytokine production and immunogenic cell death in cancer cells. Activation of RIG-I in a number of cancer cell types, including melanoma, lung, breast, and prostate cancer cell lines, has been shown to increase tumor immunogenicity via several interconnected mechanisms, including induction of cancer cell-specific death and liberation of tumor antigen, production of anti-tumor cytokines and T cell chemokines, and increased expression of MHC-I.[35, 39, 55-59] We first evaluated the ability of NP/3pRNA to enhance IFN-α secretion in several murine cell lines commonly used in pre-clinical modeling of poorly immunogenic tumors, including CT26 colon carcinoma, B16-F10 melanoma, Lewis lung carcinoma (LLC), and 4T1 breast cancer, as well as in the murine dendritic cell line DC 2.4 (Figure 1f). NP delivery of 3pRNA increased IFN-α production in all cancer cell lines tested, with the largest fold enhancement observed in the CT26 and B16 cell lines. In addition, NP delivery of 3pRNA resulted in comparable or improved IFN-α

production over delivery of 3pRNA with Lipofectamine 2000, a commercial lipid-based transfection agent used primarily for *in vitro* nucleic acid transfections. As expected, NP delivery of 3pRNA also increased IFN-α production in DC 2.4 cells relative to controls.

Based on these findings, and in light of the modest clinical response rates to PD-1 checkpoint blockade in colorectal cancer,[60] we selected the CT26 model for subsequent investigations into how NP/3pRNA could be used to increase tumor immunogenicity. CT26 cells were treated with multiple doses of NP/OH-RNA to determine the effects of the NP itself on CT26 viability and found that NPs are not toxic at the EC$_{50}$ (Figure S5a). CT26 cells were treated with NP/3pRNA, NP/OH-RNA, empty particles (NP) or a vehicle control (PBS) at an RNA dose of 50 nM. NP/3pRNA treatment increased secretion of IFN-α (Figure 2a) and gene expression of *Ifnb1* and *Cxcl10*, the latter an ISG and critical T cell chemokine, as well as the NF-κB driven pro-inflammatory cytokines, *Il6* and *Tnfa*, whereas no
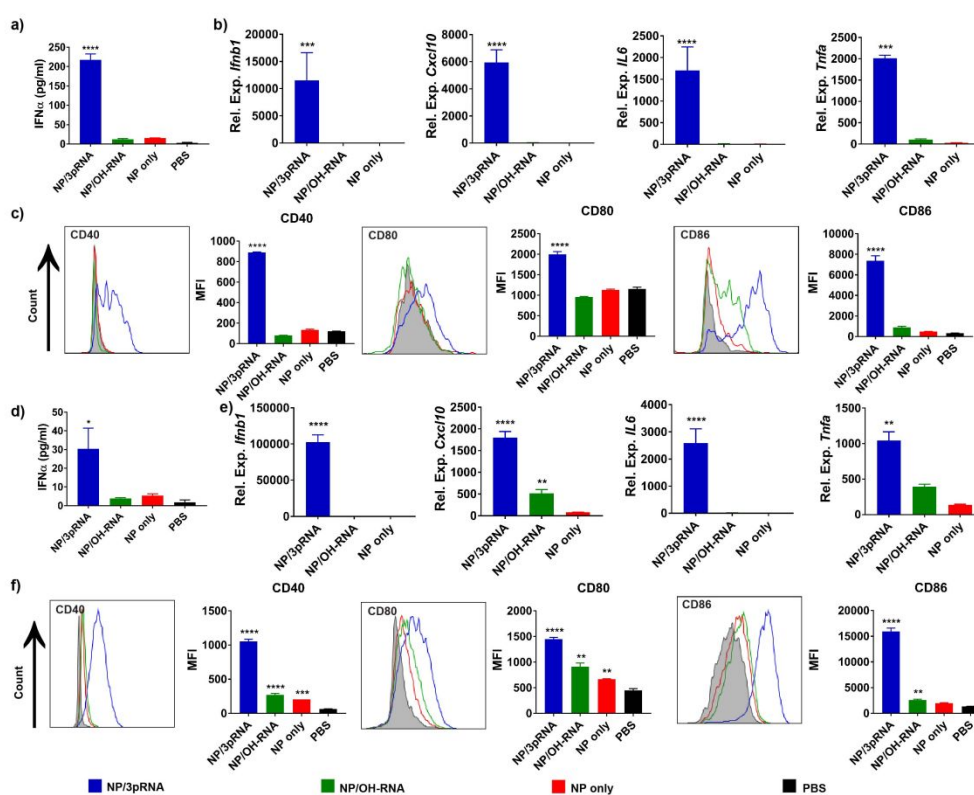
Figure 3: NP delivery of 3pRNA activates myeloid cells and induces production of inflammatory cytokines. (a) IFN-α secretion by bone-marrow derived dendritic cells (BMDCs) treated with indicated formulations (n=4). (b) Relative expression of *Ifnb1*, *Cxcl10*, *Il6*, and *Tnfa* by BMDCs measured by qRT-PCR (n=4). (c) Representative flow cytometry histograms and average median fluorescence intensity (MFI) values of CD40, CD80, and CD86 on BMDCs in response to indicated treatment (n=4). (d) IFN-α secretion by bone-marrow derived macrophages (BMDMs) treated with indicated formulations (n=4). (e) Relative expression of *Ifnb1*, *Cxcl10*, *Il6*, and *Tnfa* by BMDMs measured by qRT-PCR (n=4). (f) Representative flow cytometry histograms and average MFI values of CD40, CD80, and CD86 expression on BMDMs in response to indicated treatment (n=4). For NP/3pRNA, significance is between all other samples, and for NP/OH-RNA and NP only significance is between PBS.

increases were observed above baseline for all other groups (Figure 2b). This was further supported by protein immunoblots of CT26 cell lysates that indicated that only NP/3pRNA treatment triggered phosphorylation of IRF-3 (pIRF3), a transcription factor downstream of

RIG-I that drives expression of type-I IFN and other ISGs (Figure 2c). Additionally, NP/3pRNA resulted in phosphorylation of STAT-1, which occurs downstream of the IFN-α/β receptor, as well as increased expression of RIG-I, itself an ISG, the result of positive feedback after

initial RIG-I activation (Figure 2c). Therefore, NP delivery of 3pRNA enhances RIG-I activation in CT26 murine colon carcinoma, resulting in production of type-I IFNs and activating downstream innate immune signaling cytokines.

Previous studies have shown that RIG-I activation in several cancer cell types can lead to induction of immunogenic cell death, an inflammatory form of cell death that has been harnessed to enhance antitumor immunity.[38, 61-64] In order to determine if NP-mediated RIG-I activation could induce immunogenic cell death in CT26 colon carcinoma, cells were treated with NP/3pRNA, NP/OH-RNA, NP only, or PBS at a final RNA concentration of 50 nM for 24 hr. Protein immunoblots of cell lysates indicate that only NP/3pRNA treatment increased caspase 3 and caspase 8 cleavage (Figure 2d), indicated by the appearance of a new lower molecular weight band and decreased intensity of the characteristic caspase 3 and caspase 8 bands, which have been previously implicated in RIG-I- and type 1 IFN-dependent cancer cell death pathways. To evaluate cell viability and apoptosis in response to treatments, cells were stained with annexin-V antibodies and a 7AAD membrane permeability stain and characterized using flow cytometry to determine the percentage of

double negative (-/-), annexin-V positive (+/-), 7AAD positive (-/+), and double positive cells (+/+) (Figure 2e). Treatment with NP/3pRNA significantly reduced cell viability relative to all other groups, with a high population of Annexin-V/7AAD double positive cells, indicating a combination of necrotic and apoptotic cell death mechanisms, which is typically more immunogenic than death solely by apoptosis.[64] Additionally, NP/3pRNA resulted in evaluated surface expression of calreticulin, a marker of immunogenic cell death that promotes tumor cell phagocytosis by macrophages (Figure 2f) and secretion of HMGB1, which engages TLR-4 (Figure 2g). Collectively, these data demonstrate that NP delivery of 3pRNA can increase tumor-intrinsic activation of anti-tumor innate immunity and elicit immunogenic cell death, responses with potential to act cooperatively to enhance anti-tumor adaptive immunity.

NP delivery of 3pRNA activates primary dendritic cells and macrophages. A variety of different cell populations contribute to propagating immunosuppression in the TME, and therefore immunotherapeutics that are able modulate the immunophenotype of multiple cell types may be more effective for increasing tumor immunogenicity.[8, 11, 65] Tumor infiltrating myeloid cell populations,
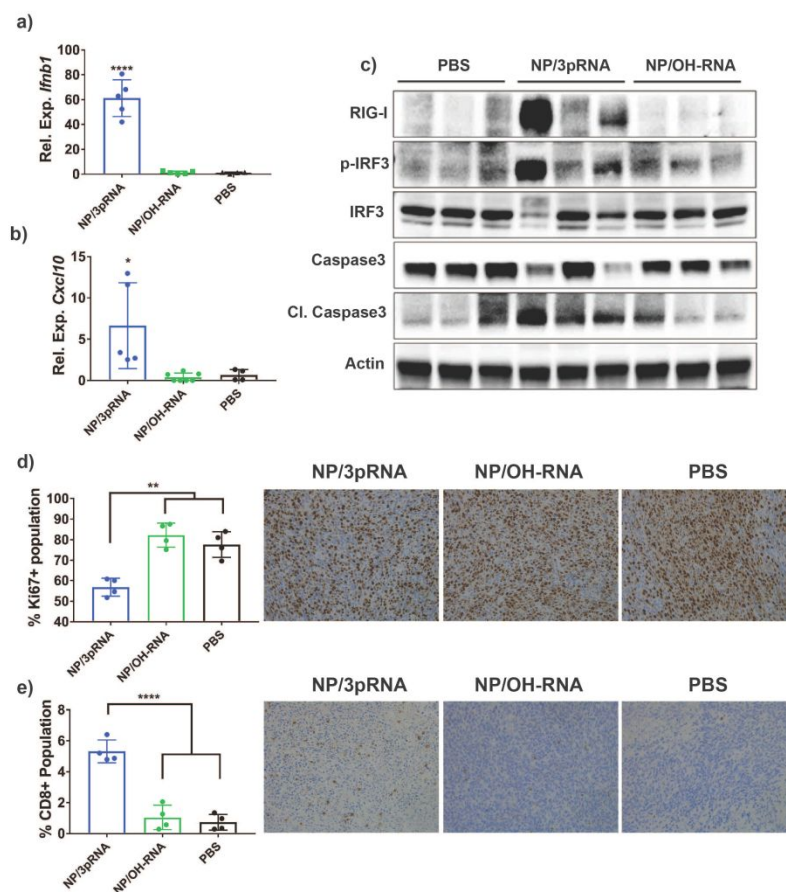
Figure 4: NP delivery of 3pRNA activates RIG-I in CT-26 tumors and increases CD8+ T cell infiltration. Gene expression of a) *Ifnb1* and b) *Cxcl10* in CT26 tumors treated with indicated formulation was determined using qRT-PCR (n=4). c) Treated tumors were analyzed using a protein immunoblot to determine relative expression of RIG-I, phosphorylated IRF3 (pIRF3), and cleaved caspase 3 (n=3). (d) Sections from CT26 tumors injected with indicated formulation were immunostained for Ki67 and the percentage of Ki67+ was quantified by image analysis (n=4). (e)

Biomaterials Science ARTICLE

Sections from CT26 tumors injected with indicated formulation were immunostained for CD8 and the percentage of CD8^{+} was quantified by image analysis (n=4).

including tumor-associated macrophages, myeloid derived suppressor cells, and dendritic cells, are important cell populations in regulating the balance between immunosuppression and effective anti-tumor immunity.[8] We therefore evaluated the capacity of NP/3pRNA to activate RIG-I and trigger anti-tumor innate immune response in bone marrow derived dendritic cells (BMDCs) and bone marrow derived macrophages (BMDMs). As described above, both primary cell types were treated with NP/3pRNA, NP/OH-RNA, NP only, or PBS at a final RNA concentration of 50 nM.

We first evaluated the ability of NP/3pRNA to activate BMDCs. Treatment of BMDCs with NP/3pRNA stimulated expression (*Ifnb1*) and secretion (IFN-α) of type I IFN, as well as expression of *Cxcl10* and the pro-inflammatory cytokines *Il6* and *Tnfa* whereas no increase above background was observed for all control groups (Figure 3a,b). We further analyzed BMDC activation using flow cytometry to measure surface expression of co-stimulatory molecules (Figure 3c). Consistent with gene expression data, only NP/3pRNA resulted in increased expression of CD40 (9-fold), CD80 (2-fold), and CD86 (23-fold).

We next evaluated the ability of NP/3pRNA to activate BMDMs. Results were largely similar to those obtained in BMDCs, with only NP/3pRNA activating production of type-I IFN, IL-6, and TNFα (Figure 3d,e). NP/OH-RNA resulted in a slight, but statistically significant, increase in *Cxcl10* expression, potentially a result of intrinsic inflammatory properties of the RNA/NP complex in macrophages. Similarly, surface expression of CD86, CD40, and CD80 were most significantly increased in response to NP/3pRNA (Figure 3f), though a small but significant increase over background was observed for NP/OH-RNA and NP, potentially reflecting some inherent immunostimulatory properties of the NP, as has been previously described for other cationic and/or endosomolytic materials.[66-69] These effects did not appear to be a result of polymer toxicity, as treatment of DC 2.4 and RAW 264.7 cells with relevant concentrations of NP/OH-RNA did not result in cytotoxicity (Figure S5b, S5c). Nonetheless, these data collectively demonstrate that NPs enhance the delivery of 3pRNA to primary macrophages and DCs, resulting in activation of RIG-I and downstream stimulation of type-I IFN, ISGs, and pro-inflammatory cytokines. Given the immunosupressive capacity of TAMs in many tumor types as well as the importance of DC activation in priming of anti-tumor adaptive immunity and memory responses, these results further support application of NP/3pRNA-mediated activation of RIG-I to increase tumor immunogenicity and improve outcomes of cancer immunotherapy.
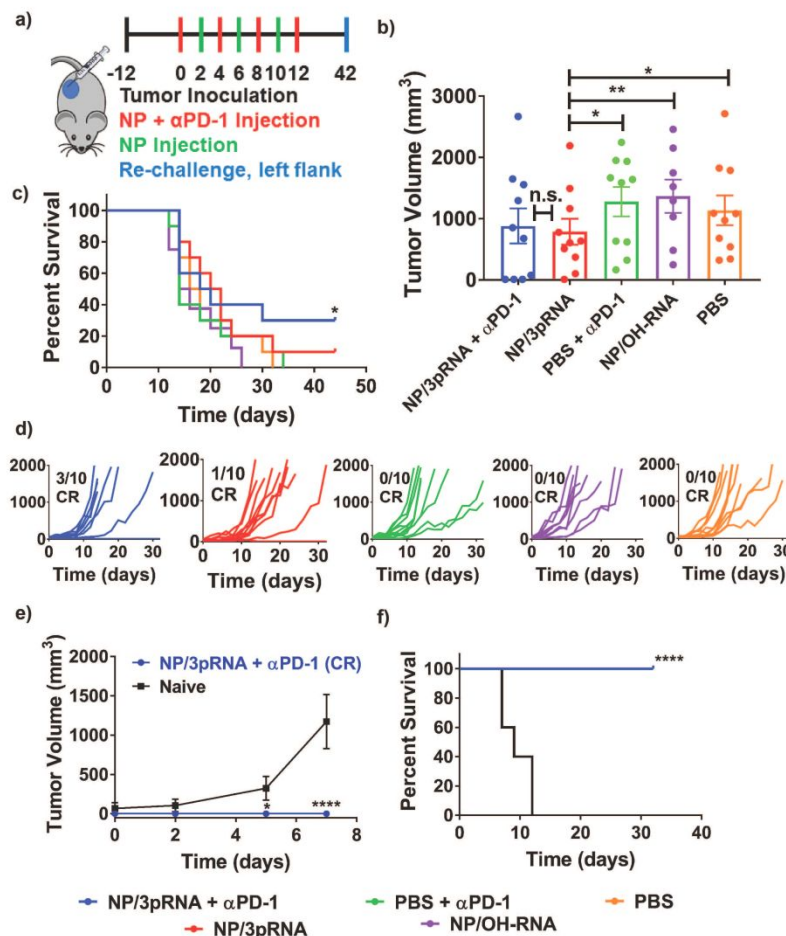
Figure 5: NP delivery of 3pRNA in combination with αPD-1 inhibits tumor growth and extends survival. (a) Schematic summarizing tumor formation and treatment schedule used for evaluating efficacy of NP/3pRNA in combination with PD-1 blockade. Mice bearing CT26 tumors were treated intratumorally 5 times spaced two days apart (IT) with NP/3pRNA, NP/OH-RNA, or PBS. Mice were injected with αPD-1 every 4 days intraperitoneally. Mice demonstrating complete responses were challenged on the contralateral flank with CT26 tumor cells on day 42. (b) Average tumor volume at day 14, corresponding to the first incidence of euthanize in any treatment or control cohort. Error bars represent S.D. (c) Kaplan-Meier survival curves of mice treated with indicated formulation using 1500 mm³ tumor volume as endpoint criteria (n=10). (d) Spider plots of individual growth curves with the number of complete responses (CR) at day 42 denoted. (e) Mice exhibiting CRs to NP/3pRNA + αPD-1 treatment were rechallenged with CT26 cells on the contralateral flank without further treatment and tumor growth was compared to treatment-naïve mice inoculated with CT26 cells. Tumor measurements begin two weeks after tumor rechallenge/inoculation, when tumors became palpable (n=3 for CR mice, n=5 for naïve mice). Significance was determined for day 7 between naïve and Cr mice. (f) Kaplan-Meier survival curves for treatment naïve and CRs to NP/3pRNA + αPD-1. Significance was determined using two-way ANOVA with Tukey's multiple comparisons test. Significance for survival was determined using a Mantel-Cox log-rank test.

NP delivery of 3pRNA activates RIG-I in CT-26 tumors and increases CD8+ T cell infiltration. We next evaluated the ability of NP/3pRNA to activate anti-tumor innate immunity in CT26 tumors. Mice with subcutaneous (SC) CT26 tumors were administered NP/3pRNA, NP/OH-RNA, or vehicle (PBS) two times, spaced two days apart via an intratumoral (IT) injection route. Mice did not exhibit weight loss during this treatment, indicating that IT administration of NP/3pRNA results in minimal immune-related adverse events or toxicity (Figure S6a). Mice were euthanized 24 h after the final injection, and tumors analyzed via qRT-PCR, western blot analysis, and immunohistochemical staining. IT administration of NP/3pRNA significantly increased expression of *Ifnb1* and *Cxcl10* (Figure 4a,b), whereas no increase above baseline was observed for NP/OH-RNA. Likewise, western blot analysis demonstrated increased levels of RIG-I and pIRF-3, as well as increased cleavage of caspase 3 (Figure 4c) relative to NP/OH-RNA and vehicle control, further supporting the ability of the NP to enhance cytosolic 3pRNA delivery. Consistent with increased cleaved caspase 3 levels, NP/3pRNA also inhibited cell proliferation as determined by Ki67 staining of tumor sections (Figure 4d). Importantly, immunohistochemical analysis also

revealed a significant increase in CD8 staining, likely reflecting infiltration of CD8$^+$ T cells into the TME, consistent with increased expression of *Cxcl10*, an important T cell chemokine (Figure 4e). While further investigation is necessary to understand the mechanism by which NP/3pRNA activates RIG-I to remodel the TME, these findings demonstrate the ability to leverage endosomolytic NPs to enhance 3pRNA delivery *in vivo*.

NP delivery of 3pRNA increases response rates to PD-1 checkpoint blockade in CT-26 model of colon cancer. Based on the capacity of NP/3pNRNA to stimulate RIG-I activation in the TME, we next sought to demonstrate the ability of NP/3pRNA to inhibit tumor growth and synergize with αPD-1 ICB. We evaluated this using an IT administration route that is being explored in clinical trials of immune agonists (e.g., NCT02423863, NCT02834052, NCT01984892, NCT01349959, NCT01928576), including RIG-I agonists.[33, 70] BALB/cJ mice bearing subcutaneous CT26 tumors were administered NP/3pRNA or control formulations IT every two days over a two-week period with and without concurrent systemic intraperitoneal treatment with αPD-1 monoclonal antibody (Figure 5a). NP/OH-RNA, αPD-1, and vehicle (PBS) were administered as controls. IT administration of NP/3pRNA resulted in a modest but significant reduction in tumor volume relative to αPD-1 alone, NP/control, and vehicle control, and administration of NP/3pRNA + αPD-1 did not result in significantly reduce tumor volume compared to NP/3pRNA treatment (Figure 5b). In addition, NP/3pRNA administration reduced the average doubling time of CT26 tumors compared to αPD-1 alone, NP/control, and vehicle control (Figure S7). Importantly, mice did not exhibit weight loss during or after treatment, indicating that IT administration of NP/3pRNA alone or in combination with PD-1 ICB resulted in minimal immune-related adverse effects or toxic effects (Figure S6b). While the overall effect on average tumor growth was modest, the therapeutic effect of NP/3pRNA was considerably more evident in its ability to decrease the average doubling time of CT26 tumors (Table S2) and overall rates of survival when combined with αPD-1 ICB (Figure 5c). Thirty percent (3/10) of mice treated with NP/3pRNA in combination with αPD1 demonstrated complete responses without any evidence of tumor growth for 42 days after cessation of treatment, whereas only 10% (1/10) mice receiving NP/3pRNA monotherapy and none of the mice in control cohorts exhibited complete responses (Figure 5d). To determine if this treatment regimen could stimulate adaptive immunity to protect against tumor recurrence, mice exhibiting complete responses were rechallenged with CT26 cells on the opposite flank. Without any additional treatment, rechallenged mice resisted tumor growth for at least 40 days, whereas age-matched, treatment-naïve controls succumbed to disease within 12 days (Figure 5e). While the immunological mechanisms underlying this response remain to be elucidated, these data provide the first demonstration that carrier-enhanced delivery of a 3pRNA RIG-I agonist can serve as an *in situ* vaccine that can protect against rechallenge.

Conclusions

The recent clinical success of immune checkpoint blockade has provided a clear testament to the potential for immunotherapies to revolutionize cancer treatment. Importantly, with the increased use of ICB in the clinic, a deeper understanding has also emerged as to why some patients respond remarkably to ICB, whereas most do not. This includes a greater appreciation for the importance of the innate immune system in eliciting and supporting effective anti-tumor T cell immunity, which has prompted the expansion of the immunotherapeutic armamentarium to include innate immune agonists. Within this emergent family of immunomodulators, 3pRNA agonists of RIG-I hold considerable promise owing to the robust and ubiquitous expression pattern of RIG-I, their capacity to stimulate a strong type-I IFN-driven inflammatory program, and their ability to induce immunogenic cell death in multiple cancer cell types. However, the clinical potential of 2p- and 3pRNA therapeutics remains limited by critical drug delivery challenges, including poor cellular uptake, susceptibility to nuclease degradation, and very low cytosolic bioavailability. Here, we have demonstrated that polymeric nanoparticles with pH-responsive, endosome-releasing activity can enhance the intracellular delivery of 3pRNA to potently activate the RIG-I pathway. Moreover, since a structurally analogous, but non-pH-responsive carrier did not enhance activity, our data highlights the importance of an active endosomal escape mechanism in the design of delivery systems for 3pRNA. This work also demonstrates the utility of NPs for 3pRNA delivery, with data indicating that NP/3pRNA can trigger RIG-I signaling and downstream immunostimulatory effects in macrophages, dendritic cells, and several cancer cell lines in a 3pRNA-dependent manner. Importantly, NPs enhanced activity of 3pRNA *in vivo*, stimulating expression of type I IFN and ISGs upon intratumoral administration and increasing the infiltration of CD8$^+$ T cells. Consequently, treatment with NP/3pRNA enhanced the therapeutic efficacy of αPD-1 ICB to yield significant improvement in survival and resulted in a 30% complete response rate in a CT26 murine colon cancer model. While NP properties, RIG-I ligand design, and NP/3pRNA dose and treatment regimen remain to be optimized for maximum therapeutic benefit, these studies demonstrate the importance of carrier design in immunotherapeutic targeting of the RIG-I pathway and set the stage for future investigation into the development of new delivery technologies for this promising class of innate immune agonist.

Conflicts of interest

There are no conflicts to declare.

Acknowledgements

Notes and references

1. A. Ribas and J. D. Wolchok, *Science*, 2018, **359**, 1350-1355.
2. S. L. Topalian, C. G. Drake and D. M. Pardoll, *Cancer Cell*, 2015, **27**, 450-461.
3. P. Sharma and J. P. Allison, *Cell*, 2015, **161**, 205-214.
4. P. Gotwals, S. Cameron, D. Cipolletta, V. Cremasco, A. Crystal, B. Hewes, B. Mueller, S. Quaratino, C. Sabatos-Peyton, L. Petruzzelli, J. A. Engelman and G. Dranoff, *Nat Rev Cancer*, 2017, **17**, 286-301.
5. M. A. Postow, M. K. Callahan and J. D. Wolchok, *Journal of clinical oncology*, 2015, **33**, 1974.
6. N. McGranahan, A. J. Furness, R. Rosenthal, S. Ramskov, R. Lyngaa, S. K. Saini, M. Jamal-Hanjani, G. A. Wilson, N. J. Birkbak and C. T. Hiley, *Science*, 2016, **351**, 1463-1469.
7. R. Zappasodi, T. Merghoub and J. D. Wolchok, *Cancer Cell*, 2018, **33**, 581-598.
8. M. Binnewies, E. W. Roberts, K. Kersten, V. Chan, D. F. Fearon, M. Merad, L. M. Coussens, D. I. Gabrilovich, S. Ostrand-Rosenberg, C. C. Hedrick, R. H. Vonderheide, M. J. Pittet, R. K. Jain, W. Zou, T. K. Howcroft, E. C. Woodhouse, R. A. Weinberg and M. F. Krummel, *Nat Med*, 2018, **24**, 541-550.
9. D. S. Chen and I. Mellman, *Nature*, 2017, **541**, 321-330.
10. A. Iwasaki and R. Medzhitov, *Nat Immunol*, 2004, **5**, 987-995.
11. K. D. Moynihan and D. J. Irvine, *Cancer Res*, 2017, **77**, 5215-5221.
12. L. Corrales, V. Matson, B. Flood, S. Spranger and T. F. Gajewski, *Cell Res*, 2017, **27**, 96-108.
13. D. L. Elion and R. S. Cook, *Oncotarget*, 2018, **9**, 29007-29017.
14. A. Mullard, *Nat Rev Drug Discov*, 2018, **17**, 3-5.
15. S. Gordon, *Cell*, 2002, **111**, 927-930.
16. P. Kamath, E. Darwin, H. Arora and K. Nouri, *Clin Drug Investig*, 2018, DOI: 10.1007/s40261-018-0681-x.
17. J. D. Campbell, *Methods Mol Biol*, 2017, **1494**, 15-27.
18. K. Iribarren, N. Bloy, A. Buque, I. Cremer, A. Eggermont, W. H. Fridman, J. Fucikova, J. Galon, R. Spisek, L. Zitvogel, G. Kroemer and L. Galluzzi, *Oncoimmunology*, 2016, **5**, e1088631.
19. M. Kiss, S. Van Gassen, K. Movahedi, Y. Saeys and D. Laoui, *Cell Immunol*, 2018, **330**, 188-201.
20. R. Barbalat, S. E. Ewald, M. L. Mouchess and G. M. Barton, *Annual review of immunology*, 2011, **29**, 185-214.
21. X. Cao, *Nat Rev Immunol*, 2016, **16**, 35-50.
22. L. Zitvogel, L. Galluzzi, O. Kepp, M. J. Smyth and G. Kroemer, *Nature Reviews Immunology*, 2015, **15**, 405.
23. A. Sistigu, T. Yamazaki, E. Vacchelli, K. Chaba, D. P. Enot, J. Adam, I. Vitale, A. Goubar, E. E. Baracco and C. Remédios, *Nature medicine*, 2014, **20**, 1301.
24. G. Kassiotis and J. P. Stoye, *Nature Reviews Immunology*, 2016, **16**, 207.
25. K. B. Chiappinelli, P. L. Strissel, A. Desrichard, H. Li, C. Henke, B. Akman, A. Hein, N. S. Rote, L. M. Cope and A. Snyder, *Cell*, 2015, **162**, 974-986.
26. D. Goubau, M. Schlee, S. Deddouche, A. J. Pruijssers, T. Zillinger, M. Goldeck, C. Schuberth, A. G. Van der Veen, T. Fujimura and J. Rehwinkel, *Nature*, 2014, **514**, 372.
27. M. M. Linehan, T. H. Dickey, E. S. Molinari, M. E. Fitzgerald, O. Potapova, A. Iwasaki and A. M. Pyle, *Science Advances*, 2018, **4**, e1701854.
28. V. Hornung, J. Ellegast, S. Kim, K. Brzózka, A. Jung, H. Kato, H. Poeck, S. Akira, K. K. Conzelmann, M. Schlee, S. Endres and G. Hartmann, *Science*, 2006, **314**, 994-997.
29. A. Schmidt, T. Schwerd, W. Hamm, J. C. Hellmuth, S. Cui, M. Wenzel, F. S. Hoffmann, M.-C. Michallet, R. Besch, K.-P. Hopfner, S. Endres and S. Rothenfusser, *Proceedings of the National Academy of Sciences of the United States of America*, 2009, **106**, 12067-12072.
30. R. C. Ireton and M. Gale Jr, *Viruses*, 2011, **3**, 906-919.
31. A. Kohlway, D. Luo, D. C. Rawling, S. C. Ding and A. M. Pyle, *EMBO reports*, 2013, **14**, 772-779.
32. V. Hornung and E. Latz, *Nature reviews. Immunology*, 2010, **10**, 123-130.
33. J. G. van den Boorn and G. Hartmann, *Immunity*, 2013, **39**, 27-37.
34. K. Hatano, Y. Nakai, T. Matsushima-Miyagi, M. Nomura, W. Nakata, T. Yoshida, M. Sato, A. Kawashima, A. Nagahara and K. Fujita, *Journal*, 2013.
35. R. Besch, H. Poeck, T. Hohenauer, D. Senft, G. Häcker, C. Berking, V. Hornung, S. Endres, T. Ruzicka and S. Rothenfusser, *The Journal of clinical investigation*, 2009, **119**, 2399-2411.
36. P. Duewell, A. Steger, H. Lohr, H. Bourhis, H. Hoelz, S. Kirchleitner, M. Stieg, S. Grassmann, S. Kobold and J. Siveke, *Cell death and differentiation*, 2014, **21**, 1825.
37. T. O. Kabilova, A. V. Sen'kova, V. P. Nikolin, N. A. Popova, M. A. Zenkova, V. V. Vlassov and E. L. Chernolovskaya, *PloS one*, 2016, **11**, e0150751.
38. A. Szabo, T. Fekete, G. Koncz, B. V. Kumar, K. Pazmandi, Z. Foldvari, B. Hegedus, T. Garay, A. Bacsi and E. Rajnavolgyi, *Cellular signalling*, 2016, **28**, 335-347.
39. H. Poeck, R. Besch, C. Maihoefer, M. Renn, D. Tormo, S. S. Morskaya, S. Kirschnek, E. Gaffal, J. Landsberg, J. Hellmuth, A. Schmidt, D. Anz, M. Bscheider, T. Schwerd, C. Berking, C. Bourquin, U. Kalinke, E. Kremmer, H. Kato, S. Akira, R. Meyers, G. Häcker, M. Neuenhahn, D. Busch, J. Ruland, S. Rothenfusser, M. Prinz, V. Hornung, S. Endres, T. Tüting and G. Hartmann, *Nature Medicine*, 2008, **14**, 1256-1263.
40. R. Kanasty, J. R. Dorkin, A. Vegas and D. Anderson, *Nature materials*, 2013, **12**, 967-977.
41. D. W. Pack, A. S. Hoffman, S. Pun and P. S. Stayton, *Nature Reviews Drug Discovery*, 2005, **4**, 581-593.
42. K. J. Kauffman, M. J. Webber and D. G. Anderson, *J Control Release*, 2016, **240**, 227-234.
43. K. A. Hajj and K. A. Whitehead, *Nature Reviews Materials*, 2017, **2**, 17056.
44. J. Ellermeier, J. Wei, P. Duewell, S. Hoves, M. R. Stieg, T. Adunka, D. Noerenberg, H. J. Anders, D. Mayr, H. Poeck, G. Hartmann, S. Endres and M. Schnurr, *Cancer Research*, 2013, **73**, 1709-1720.
45. J. T. Wilson, S. Keller, M. J. Manganiello, C. Cheng, C.-C. Lee, C. Opara, A. Convertine and P. S. Stayton, *ACS nano*, 2013, **7**, 3912-3925.
46. A. J. Convertine, D. S. W. Benoit, C. L. Duvall, A. S. Hoffman and P. S. Stayton, *Journal of Controlled Release*, 2009, **133**, 221-229.
47. A. J. Convertine, C. Diab, M. Prieve, A. Paschal, A. S. Hoffman, P. H. Johnson and P. S. Stayton, *Biomacromolecules*, 2010, **11**, 2904-2910.
48. C. L. Duvall, A. J. Convertine, D. S. W. Benoit, A. S. Hoffman and P. S. Stayton, *Molecular Pharmaceutics*, 2010, **7**, 468-476.
49. S. Keller, J. T. Wilson, G. I. Patilea, H. B. Kern, A. J. Convertine and P. S. Stayton, *Journal of Controlled Release*, 2014, **191**, 24-33.
50. J. T. Wilson, S. Keller, M. J. Manganiello, C. Cheng, C.-C. Lee, C. Opara, A. Convertine and P. S. Stayton, *ACS Nano*, 2013, **7**, 3912-3925.
51. M. Ferritto and D. Tirrell, 1992.
52. C. R. Palmer, M. E. Jacobson, O. Fedorova, A. M. Pyle and J. T. Wilson, *Bioconjug Chem*, 2018, **29**, 742-747.
53. M. M. Tomayko and C. P. Reynolds, *Cancer chemotherapy and pharmacology*, 1989, **24**, 148-154.
54. C. E. Nelson, J. R. Kintzing, A. Hanna, J. M. Shannon, M. K. Gupta and C. L. Duvall, *ACS nano*, 2013, **7**, 8870-8880.
55. D. Yuan, M. Xia, G. Meng, C. Xu, Y. Song and J. Wei, *Oncotarget*, 2015, **6**, 29664.
56. J. Ellermeier, J. Wei, P. Duewell, S. Hoves, M. R. Stieg, T. Adunka, D. Noerenberg, H.-J. Anders, D. Mayr and H. Poeck, *Cancer research*, 2013, canres. 3850.2011.
57. X.-Y. Li, L.-J. Jiang, L. Chen, M.-L. Ding, H.-Z. Guo, W. Zhang, H.-X. Zhang, X.-D. Ma, X.-Z. Liu and X.-D. Xi, *Molecular cell*, 2014, **53**, 407-419.
58. K. Kübler, N. Gehrke, S. Riemann, V. Böhnert, T. Zillinger, E. Hartmann, M. Pölcher, C. Rudlowski, W. Kuhn, G. Hartmann and W. Barchet, *Cancer Research*, 2010, **70**, 5293-5304.
59. D. Li, R. P. Gale, Y. Liu, B. Lei, Y. Wang, D. Diao and M. Zhang, *Leuk Res*, 2017, **58**, 23-30.
60. J. J. Lee and E. Chu, *Clin Colorectal Cancer*, 2018, DOI: 10.1016/j.clcc.2018.06.004.
61. S. N. Schock, N. V. Chandra, Y. Sun, T. Irie, Y. Kitagawa, B. Gotoh, L. Coscoy and A. Winoto, *Cell death and differentiation*, 2017, **24**, 615.
62. A. Szabo and E. Rajnavolgyi, *American journal of clinical and experimental immunology*, 2013, **2**, 195-207.
63. R. C. Ireton and M. Gale, *Viruses*, 2011, **3**, 906-919.
64. L. Galluzzi, A. Buque, O. Kepp, L. Zitvogel and G. Kroemer, *Nat Rev Immunol*, 2017, **17**, 97-111.
65. A. O. Kamphorst, K. Araki and R. Ahmed, *Vaccine*, 2015, **33 Suppl 2**, B21-B28.
66. J. I. Andorko and C. M. Jewell, *Bioeng Transl Med*, 2017, **2**, 139-155.
67. F. Wegmann, K. H. Gartlan, A. M. Harandi, S. A. Brinckmann, M. Coccia, W. R. Hillson, W. L. Kok, S. Cole, L.-P. Ho, T. Lambe, M. Puthia, C. Svanborg, E. M. Scherer, G. Krashias, A. Williams, J. N. Blattman, P. D. Greenberg, R. A. Flavell, A. E. Moghaddam, N. C. Sheppard and Q. J. Sattentau, *Nature Biotechnology*, 2012, **30**, 883-888.

Biomaterials Science

ARTICLE

68. E. C. Carroll, L. Jin, A. Mori, N. Munoz-Wolf, E. Oleszycka, H. B. T. Moran, S. Mansouri, C. P. McEntee, E. Lambe, E. M. Agger, P. Andersen, C. Cunningham, P. Hertzog, K. A. Fitzgerald, A. G. Bowie and E. C. Lavelle, *Immunity*, 2016, **44**, 597-608.
69. S. Manna, W. J. Howitz, N. J. Oldenhuis, A. C. Eldredge, J. Shen, F. N. Nihesh, M. B. Lodoen, Z. Guan and A. P. Esser-Kahn, *ACS Central Science*, 2018, **4**, 982-995.
70. A. Marabelle, H. Kohrt, C. Caux and R. Levy, *Clinical cancer research : an official journal of the American Association for Cancer Research*, 2014, **20**, 1747-1756.

Delivery of a 5' triphosphate RNA (3pRNA), a ligand for RIG-I, with endosomolytic nanoparticles (NP) augments response to anti-PD1 immune checkpoint blockade.

80x40mm (300 x 300 DPI)